Supplementary Information

Gradient oxygen doping triggered a microscale built-in electric field in $CdIn_2S_4$ for photoelectrochemical water splitting

Jingwen Sun,‡* Shangling Han,‡ Fanglei Yao, Ruixin Li, Chenchen Fang, Xiaoyuan Zhang, Yaya Wang, Xuefeng Xu, Di Wu, Kai Liu, Pan Xiong and Junwu Zhu

Key Laboratory for Soft Chemistry and Functional Materials, Ministry of Education, Nanjing University of Science and Technology, Nanjing 210094, China

E-mail: Jingwen_Sun@njust.edu.cn

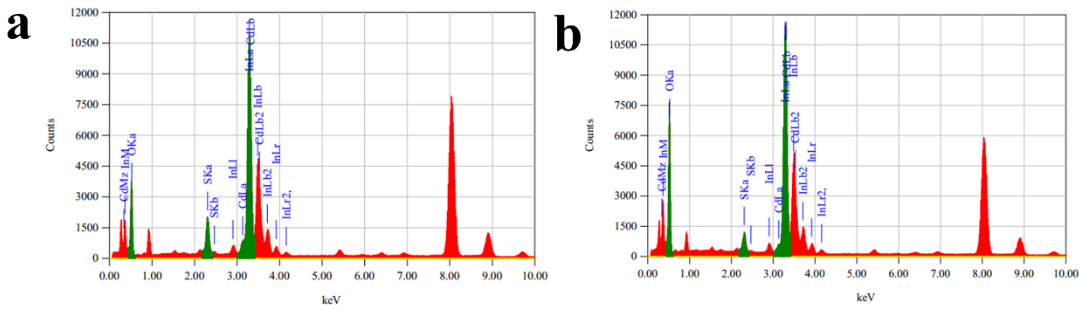

Fig. S1. The EDX spectra of (a) CIS and (b) OCIS.

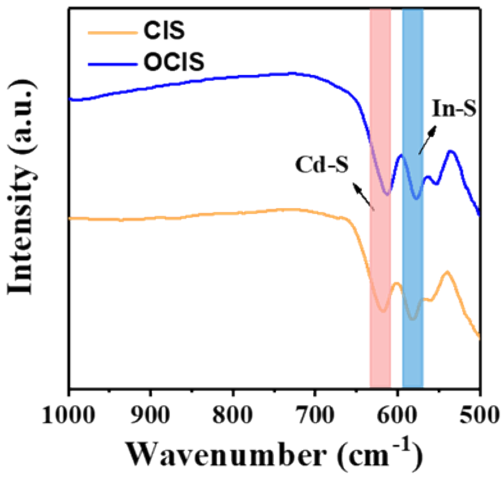

Fig. S2. The FTIR spectroscopy of CIS and OCIS.

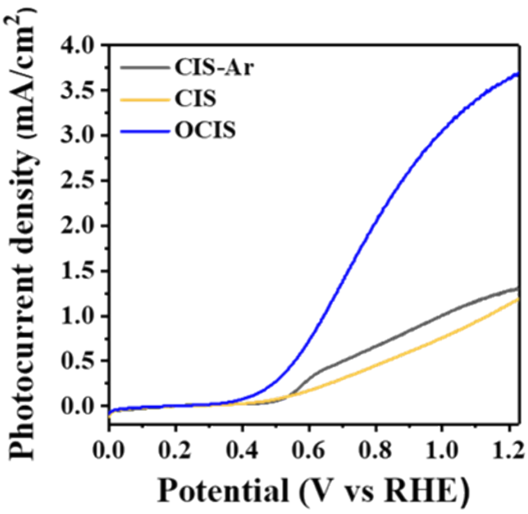

Fig. S3. LSV curves of CIS-Ar, CIS and OCIS.

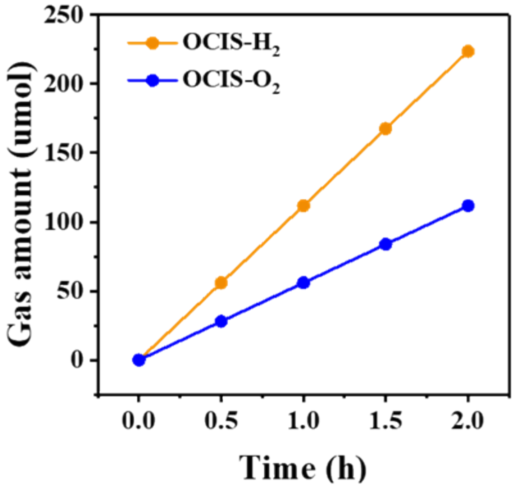

Fig. S4. Quantities of H_2 and O_2 evolution over OCIS catalyst.

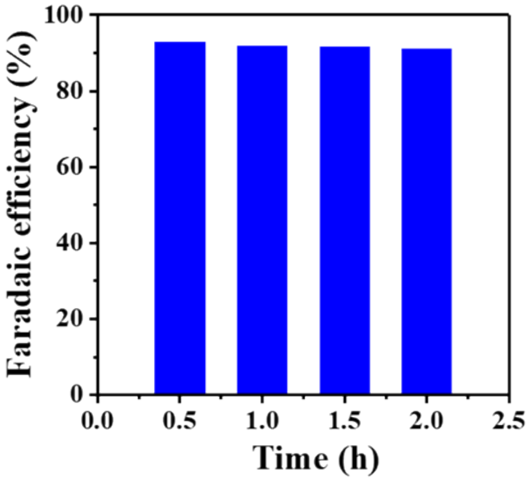

Fig. S5. Faradaic efficiencies of the O_2 production of OCIS.

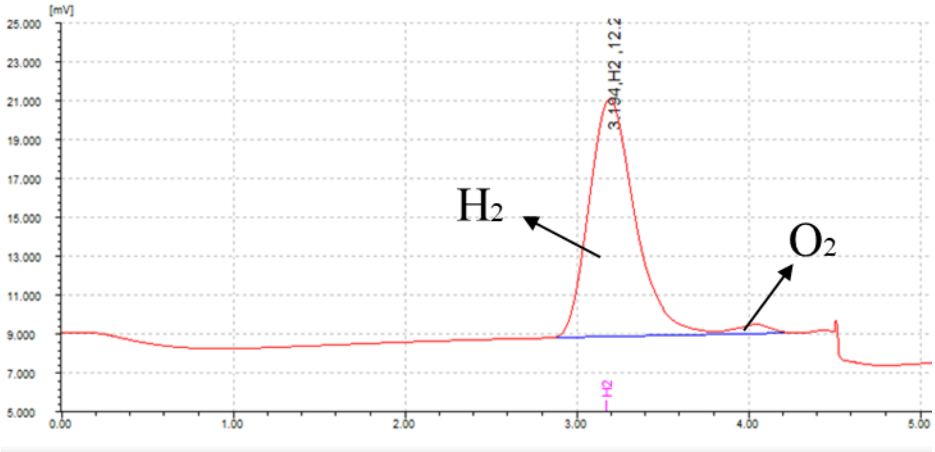

Fig. S6. Gas chromatogram of H_2 and O_2 under sacrificial agent.

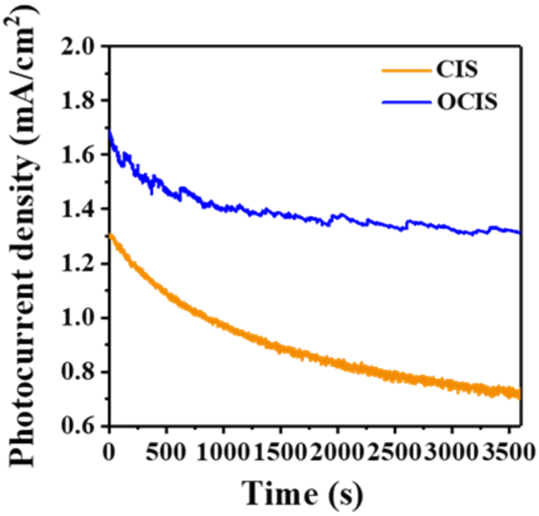

Fig. S7. Chronoamperometry tests of CIS and OCIS in the mixture of 0.25 M Na_2S and 0.35 M Na_2SO_3.

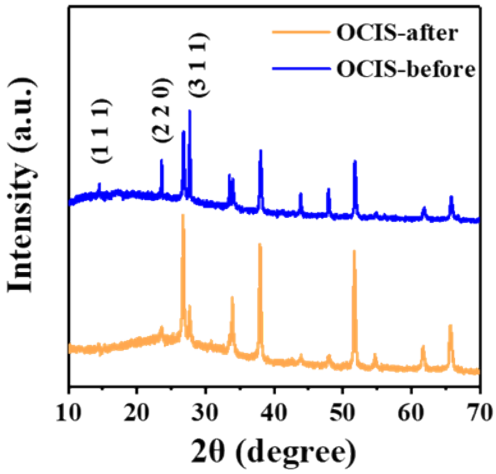

Fig. S8. XRD spectra of OCIS before and after chronoamperometry test.

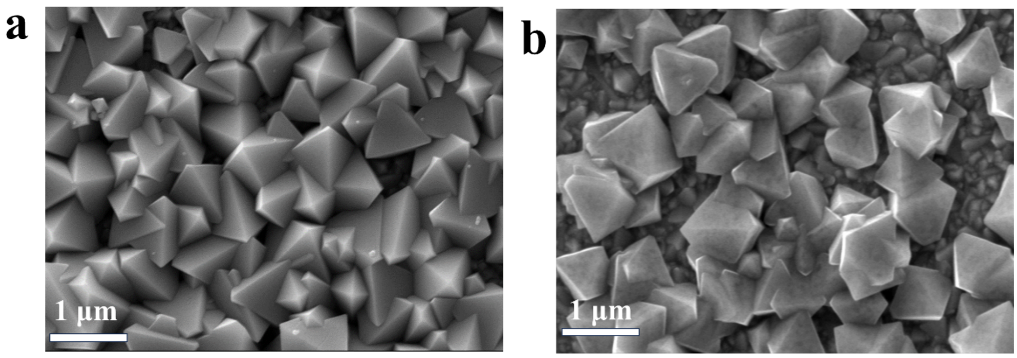

Fig. S9. The SEM images of OCIS (a) before, (b) after chronoamperometry test.

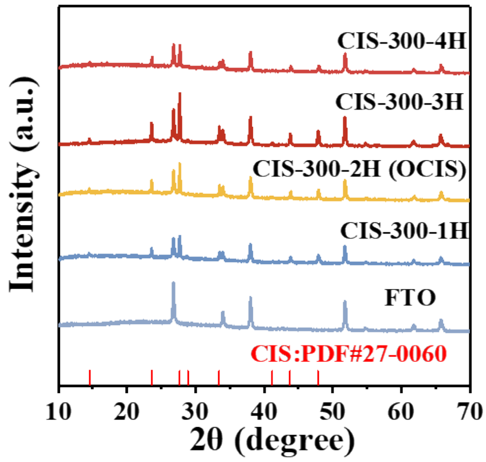

Fig. S10. XRD patterns of CIS annealed at 300 °C for different time.

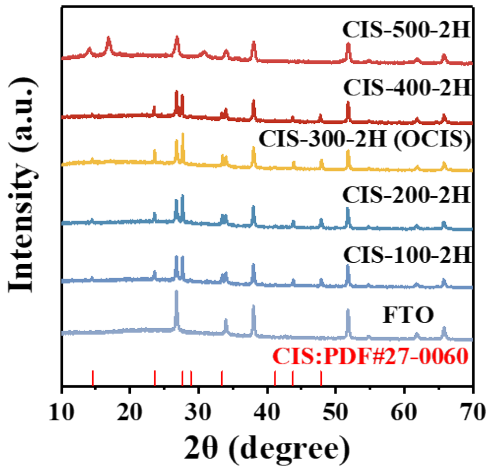

Fig. S11. XRD patterns of CIS annealed at 2 h for different temperatures.

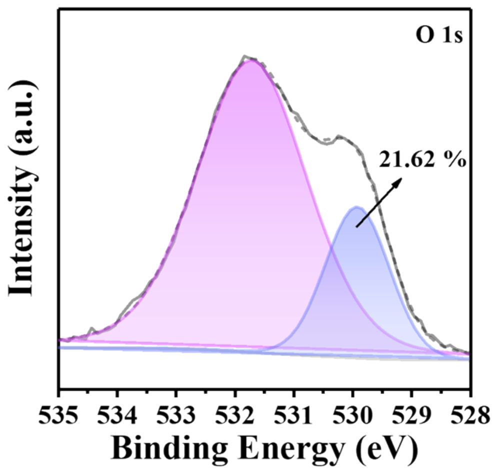

Fig. S12. The high-resolution XPS spectra of O1s in OCIS.

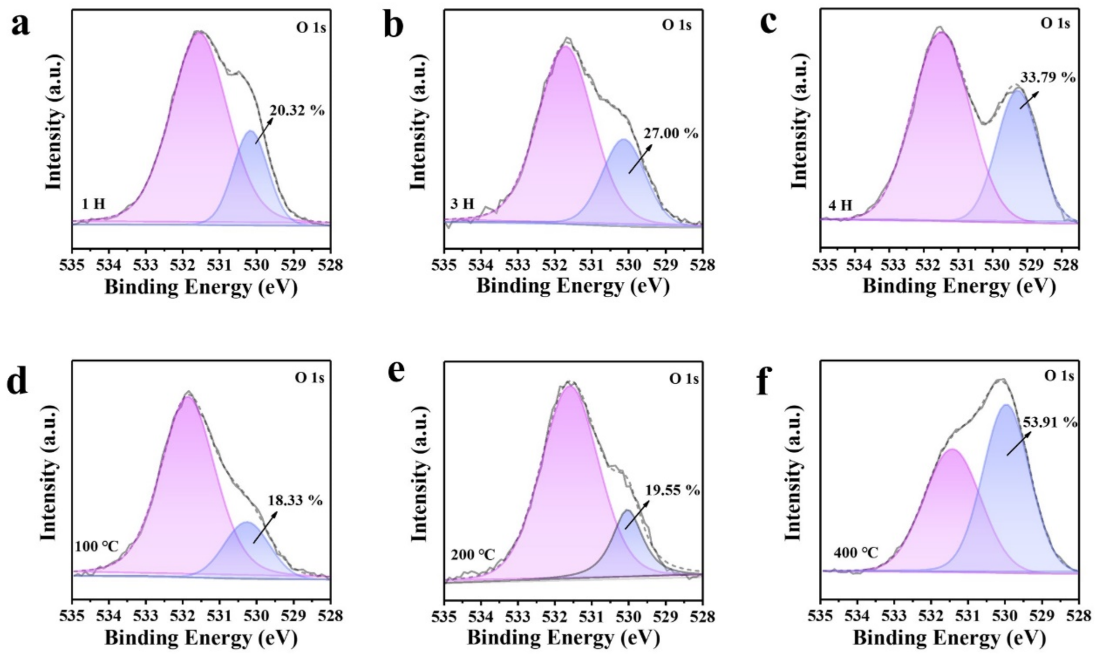

Fig. S13. The high-resolution XPS spectra of O 1s in CIS annealed at 300 °C for different time: (a) 1 h, (b) 3 h, (c) 4 h. XPS spectra of O 1s in CIS annealed for 2 h at different temperature (d) 100 °C, (e) 200 °C, (f) 400 °C.

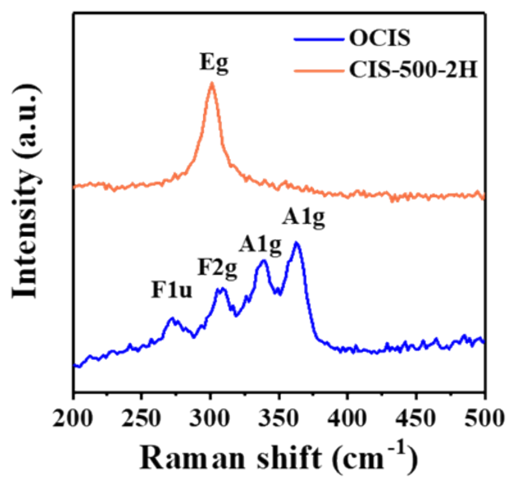

Fig. S14. Raman spectra of OCIS and CIS-500-2H.

Moreover, CIS-500-2H is further analyzed by Raman spectrum. In the range of 200-500 cm^{-1}, there is an absence of any distinctive Raman peaks associated with CIS. The characteristic peak at 301 cm^{-1} represents the stretching vibration of the Eg mode of In_2O_3 (Fig. S14). This indicates that CIS has been completely oxidized at 500 °C, which is consistent with the XRD results.

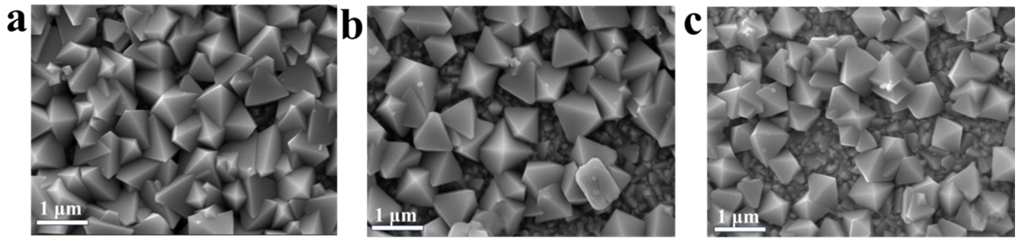

Fig. S15. The SEM images of (a) OCIS, (b) CIS-300-4H and (c) CIS-400-2H.

The morphological images of CIS-300-4H and CIS-400-2H are displayed in Fig. S15. In comparison with OCIS (Fig. S15a), even similar octahedral structure can be distinctly characterized, the homogeneity and crystallinity are more or less damaged along with the prolonged annealing time (Fig. S15b) or an increasing temperature (Fig. S15c). This phenomenon is unfavorable for the investigation of catalytic activity.

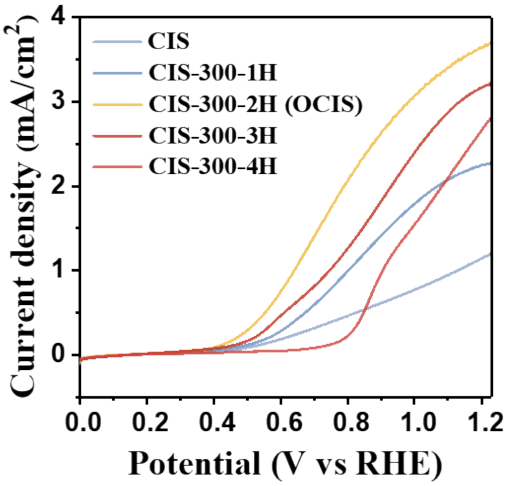

Fig. S16. LSV of CIS annealed at 300 °C for different time.

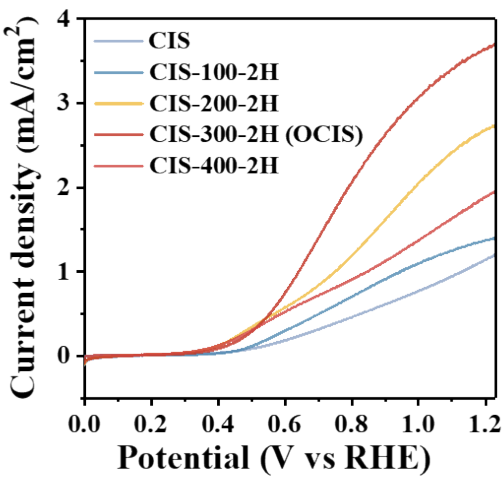

Fig. S17. LSV of CIS annealed for 2 h at different temperature.

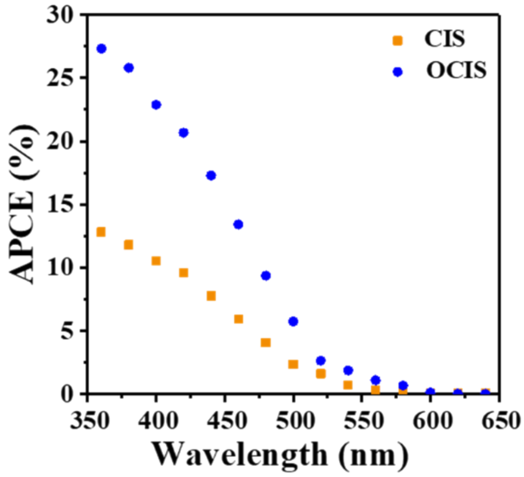

Fig. S18. The APCE of CIS and OCIS photoanodes.

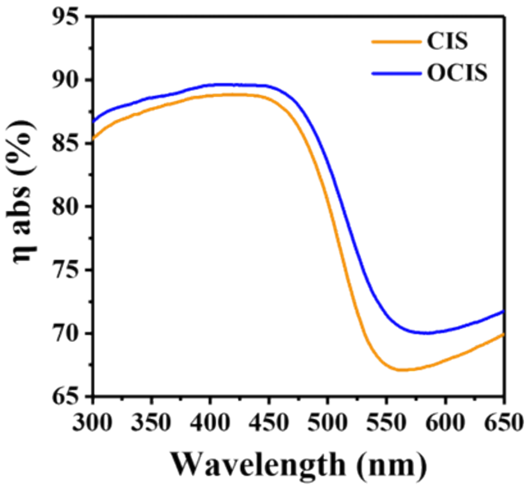

Fig. S19. Light absorption efficiency of CIS and OCIS.

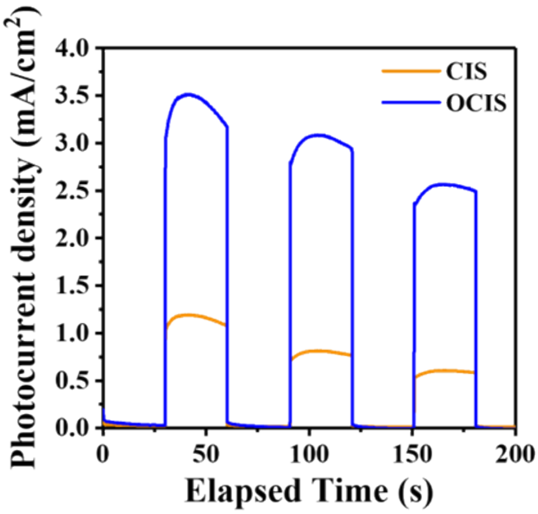

Fig. S20. Transient photocurrent response plots of CIS and OCIS.

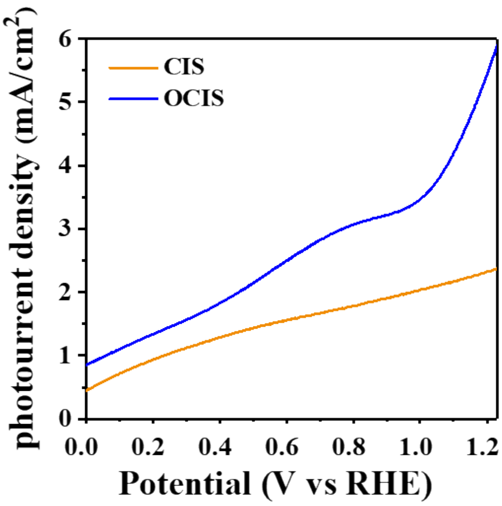

Fig. S21. LSV curves of CIS and OCIS in the mixture of 0.35 M Na_2SO_3 and 0.25 M Na_2S (pH = 12.5).

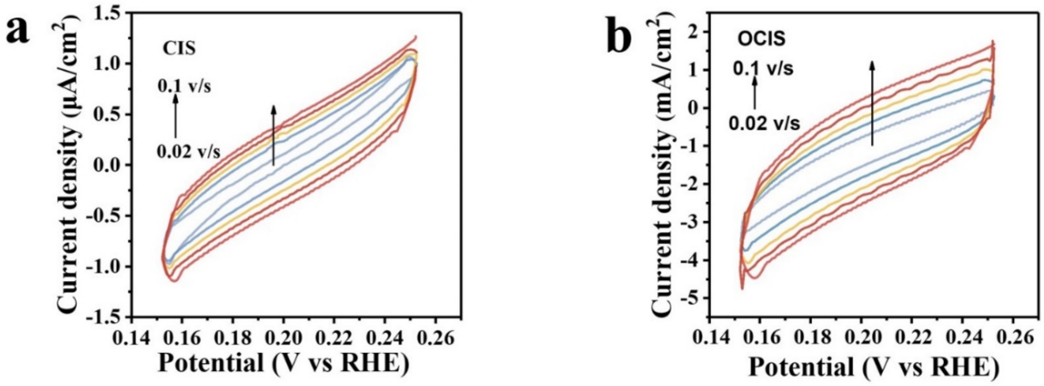

Fig. S22. Cyclic voltammogram measurements of (a) CIS and (b) OCIS at a scan rate ranging from 0.02-0.1 V/S.

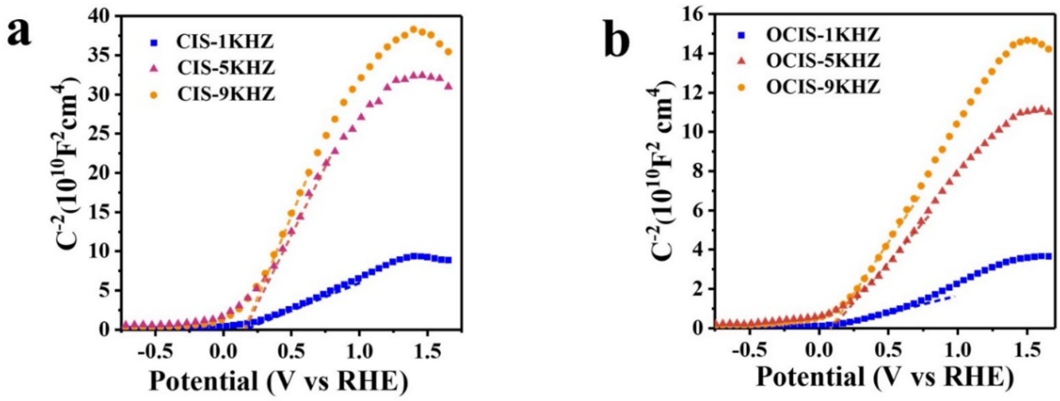

Fig. S23. M-S plots of (a) CIS and (b) OCIS in different frequencies.

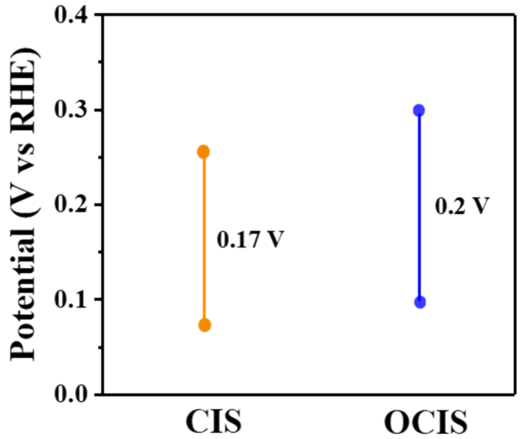

Fig. S24. OCP values of CIS and OCIS photoanodes.

Table S1. The PEC performance of reported metal sulfide based photoanodes.

Photoanode	Electrolyte	J (mA/cm^2 vs $1.23V_{RHE}$)	V_{onset} (V_{RHE})	Ref
Vs-$CdIn_2S_4$	Na_2SO_3 and Na_2S	5.73	~ -0.15	[1]
ZIS-O-S	Na_2SO_4	4.09	0.10	[2]
$ZnIn_2S_4$/CdS/ZnO	Na_2SO_4	3.48	-0.03	[3]
$CdIn_2S_4$/InOx/NiFe-LDH	KOH	5.47	~ 0.12	[4]
ZIS-O-TS	Na_2SO_4	4.57	-0.14	[5]
CIS/Ni-PPy	Na_2SO_4	6.07	0.19	[6]
$CdIn_2S_4$/In_2S_3/SnO_2	Na_2SO_4	2.98	0.02	[7]
SnS/SnS_2	Na_2SO_4	2.15	0.16	[8]
In_2S_3/TiO_2	KOH	2.71	/	[9]
WO_3/In_2S_3	Na_2SO_4	1.60	~ 0.10	[10]
O-CIS	Na_2SO_4	3.69	~ 0.19	This work

Table S2. The summary of lattice oxygen content and performance of the prepared photoanodes.

Sample	Lattice oxygen content (%)	photocurrent density (mA/cm^2)
CIS-300-1H	20.32	2.26
CIS-300-2H (OCIS)	21.62	3.62
CIS-300-3H	27.00	3.17
CIS-300-4H	53.91	2.76
CIS-100-2H	18.33	1.38
CIS-200-2H	19.55	2.71
CIS-400-2H	53.91	1.94

Table S3. The summary of fitted data from the TRPL spectra.

	A1	τ1 (ns)	A2	τ2 (ns)	τ (ns)
CIS	514.46	0.79	37.25	44.27	35.62
CIS	500.16	0.74	32.58	47.30	38.28

Table S4. The summary of EIS fitted parameters of samples under illumination.

	Rs (Ω)	Rct (kΩ)
CIS	20.8	2.5
OCIS	27.1	29.6

References

[1] H. Wang, Y. Xia, H. Li, X. Wang, Y. Yu, X. Jiao, D. Chen, Nat. Commun. 2020, 11, 3078

[2] W. Xu, W. Gao, L. Meng, W. Tian, L. Li, Adv. Energy Mater. 2021, 2101181

[3] W. Xu, W. Tian, L. Meng, F. Cao, L. Li, Adv. Energy Mater. 2021, 11, 2003500

[4] H. Wang, Y. Xia, N. Wen, Z. Shu, X. Jiao, D. Chen, Appl. Catal. B: Environ. 2022, 300, 120717

[5] L. Meng, M. Wang, H. Sun, Dr. W. Tian, Dr. F. Cao, Prof. L. Li, Adv. Energy Mater. 2022, 12, 2200629

[6] W. Xu, L. Meng, W. Tian, S. Li, F. Cao, L. Li, Small 2022, 18, 2105240

[7] L. Meng, M. Wang, H. Sun, W. Tian, C. Xiao, S. Wu, F. Cao, L. Li, Adv. Mater. 2020, 32, 2002893

[8] L. Meng, X. Zhou, S. Wang, Y. Zhou, W. Tian, P. Kidkhunthod, S. Tunmee, Y. Tang, R. Long, Y. Xin, L. Li, Angew. Chem. Int. Ed. 2019, 58, 16668

[9] J. Park, T. H. Lee, C. Kim, S. A. Lee, M. J. Choi, H. Kim, J. W. Yang, J. Lim, H. W. Jang, Appl. Catal. B: Environ. 2021, 295, 120276

[10] W. Tian, C. Chen, L. Meng, W. Xu, F. Cao, L. Li, Adv. Energy Mater. 2020, 10, 1903951